Measurements of thermodiffusion near the miscibility gap of liquid Al–In alloys

Journal of Physics: Condensed Matter

OPEN ACCESS

RECEIVED
17 November 2025

REVISED
16 January 2026

ACCEPTED FOR PUBLICATION
18 February 2026

PUBLISHED
2 March 2026

PAPER

Measurements of thermodiffusion near the miscibility gap of liquid Al–In alloys

Asbjørn Torsvik Krüger, Elke Sondermann* and Andreas Meyer

Institute of Material Physics in Space, German Aerospace Center (DLR), 51170 Cologne, Germany

* Author to whom any correspondence should be addressed.

E-mail: elke.sondermann@dlr.de

Keywords: thermodiffusion, diffusion, liquid metals

Abstract

Thermodiffusion designates a diffusive motion of particles driven by a temperature gradient. In liquid alloys this effect can influence the concentration distribution during directional solidification and change the homogeneity of grown crystals. The effect has been shown to be very strong in mixtures with a miscibility gap, due to the halting of mixing, so that the concentration separation is not held back by interdiffusion anymore, but this has until now not been observed outside of organic mixtures. Here, using x-ray radiography, thermodiffusion at the miscibility gap of liquid Al–In has been measured, with compositions ranging from $Al_{97}In_3$ to $Al_{70.5}In_{29.5}$. Closer to the miscibility gap the interdiffusion coefficient diminishes, while the thermodiffusion coefficient remains virtually unchanged, leading the ratio of the two coefficients (the so-called Soret coefficient) to diverge. This result is similar to previous investigations on liquid organic mixtures with miscibility gaps.

1. Introduction

Thermodiffusion, also called the Soret effect, describes the separation of the components of a mixture toward the hot/cold regions in a nonuniform temperature distribution [1]. The effect is observed to influence all kinds of matter, from gases, liquids, to solids [2].

Thermodiffusion is relevant in liquid alloys as their high melting points involve high temperatures and large temperature gradients. In metals, thermodiffusion can affect solders [3] and the manufacturing of integrated circuits [4], it has been employed for crystal growth [5, 6], and has recently been shown to be of use in creating metallic nanowires [7].

Through the years, several theoretical models have been proposed to predict the extent of thermodiffusion in liquid mixtures, but as we have shown in a previous work, such predictive models are not accurate for liquid alloys [8].

In previous experimental works of thermodiffusion in binary alloys, closed containers with columns of the liquid were submitted to a thermal gradient for a certain amount of time, then quickly cooled, and finally analysed in the solid state [9–11]. To avoid changes of the concentration gradient during solidification, some experiments instead used a shear cell technique, where the sample is split up into segments after the annealing time while still in the liquid state [12, 13]. A drawback of both these methods is that possible free surfaces in the melt cannot be detected, which may be caused by improper sample filling or trapped gases. Together with temperature gradients, such free surfaces may lead to Marangoni convection, which can disturb diffusion measurements [14–16]. Recently, *in situ* x-ray radiography (XRR) has been shown to allow time- and space-resolved measurements of thermodiffusion in liquid alloys, where bubbles or free surfaces can be directly detected during the experiment [17]. Using this time-resolved method it is also possible to determine the coefficients for interdiffusion and thermodiffusion simultaneously [8].

Aluminium alloys are of great importance in the industry, with a huge number of alloys of various amounts of components being in use [18, 19]. With its low atomic number, it is one of the lightest naturally occurring metals. Combined with the abundance of the element on Earth and its low reactivity, these aspects underscore its significance in various industrial contexts. Indium and alloys containing it, are especially interesting in the liquid state, as indium and generally alloys thereof have low melting points, making them applicable as agents for liquid metal cooling purposes, such as in nuclear reactors or electronic devices [20–22].

Al–In alloys are scientifically interesting due to having a miscibility gap in the liquid state between indium concentrations from 4.8 at% to 87.2 at% [23]. Also in the solid state, aluminium and indium do not dissolve into each other. The inhomogeneity caused by this makes liquid immiscible alloys of industrial interest, making it possible to utilise the different properties of the two phases of the solid alloy, such as for electrical switches and for self-lubricating bearings [24].

The coefficient for the concentration separation from thermodiffusion, the Soret coefficient, is defined as the ratio between the thermodiffusion coefficient and the interdiffusion coefficient [1]. Towards the spinodal the thermodynamic factor (TDF) approaches zero [25], and according to the Darken equation, the mixing of the components is halted as the interdiffusion approaches zero [26]. For a non-diverging, non-zero thermodiffusion coefficient, this would imply a diverging Soret coefficient when approaching the spinodal, as thermodiffusion is demixing the liquid without any interdiffusion to limit the resulting concentration separation. Whereas thermodiffusion in most mixtures leads to only a minor concentration separation [8, 27, 28], experiments on thermodiffusion in organic systems with a miscibility gap have shown the concentration separation increasing rapidly towards the critical limit [29–33]. This has so far not been investigated for any liquid alloys, although the slowing down of the interdiffusion coefficient itself towards the spinodal has been previously observed [34–36].

This study focuses on aluminium rich Al–In because for indium rich Al–In the contrast in x-ray absorption is lower leading to higher uncertainties.

2. Theory

Considering a binary mixture, the mass diffusion is driven by the interdiffusion from the concentration difference Δc, and the thermodiffusion from the temperature difference ΔT, so that at the steady state the interdiffusion and thermodiffusion processes reach an equilibrium defined by [1]

$$\Delta c_\infty = -\frac{D_\mathrm{T}}{D} c_0 \left(1 - c_0\right) \Delta T, \tag{1}$$

where c_0 is the average concentration of the mixture. The ratio between the thermodiffusion and interdiffusion coefficients (D_T and D, respectively) is called the Soret coefficient $S_\mathrm{T} \equiv \frac{D_\mathrm{T}}{D}$. The transient concentration difference between the top and the bottom of the sample is given by [37]

$$\Delta c\left(t\right) = \Delta c_\infty \left(1 - \frac{8}{\pi^2} \sum_{n=0}^{\infty} \frac{\exp\left(-\left[2n+1\right]^2 t/\theta\right)}{\left[2n+1\right]^2}\right) \tag{2}$$

where $\theta = \frac{L^2}{\pi^2 D}$ is the characteristic time, and L is the sample length.

From irreversible thermodynamics theory, the coefficients for interdiffusion and thermodiffusion can be expressed as [38, 39]

$$D = \frac{\phi L_{00} R}{\rho c_0 \left(1 - c_0\right)} \quad \text{and} \quad D_\mathrm{T} = \frac{L_{0q}}{\rho c_0 \left(1 - c_0\right) T^2}, \tag{3}$$

where L_{00} and L_{0q} are the Onsager coefficients for the heat and mass flux, ρ the mass density, R the molar gas constant, and ϕ the TDF, itself defined as [25]

$$\phi = \frac{c_i \left(1 - c_i\right)}{RT} \frac{\partial^2 G}{\partial {c_i}^2}, \tag{4}$$

where G is the Gibbs energy. The TDF describes how ideally the mixture is behaving, with $\phi = 1$ for an ideal mixture, and $\phi = 0$ at the critical point of an immiscible mixture.

When $\phi \to 0$, it leads to $D \to 0$, while D_T is independent of ϕ. Thus, with a non-zero thermodiffusion coefficient, the Soret coefficient increases.

3. Method

The general setup has been described in detail in an earlier publication [8]. It comprises a specialised furnace installed in a vacuum chamber. The furnace itself consists of a boron nitride crucible with four borings in which the samples are inserted. Resistance heaters at the upper and lower ends of the crucible make it possible to set a homogeneous temperature distribution or a temperature gradient along the sample. A piston mechanism avoids bubbles and free surfaces in the molten samples.

The borings for the sample cells containing Al–In were slightly wider than what was used in our previous thermodiffusion experiments, at 1.6 mm, to fit the wires of the pure components. For this system, wires of the pure metals were acquired (99.999% pure aluminium wire and 99.99% pure indium wire, both with 1.5 mm diameter supplied from chemPUR), and cut down and polished to lengths so that the combined metals when mixed would form alloys of desired concentration and total volume. The indium wire and the aluminium wire were stacked on top of each other in the borings of the sample cell to form a sample of about 12 mm in length.

For this work, experiments on the initial concentrations ranging from $Al_{97}In_3$ to $Al_{70}In_{30}$ were performed at mean temperatures ranging from 1014 K to 1159 K, which according to the phase diagram evaluated by Singh and Sommer should be in the region close to the miscibility gap on the Al-rich side [23]. The mean temperature of an experiment is determined by the mean of the temperatures at the top and bottom of the sample.

In the sample cell, the samples were melted while vertical, then while at a homogeneous and stable temperature, the samples were rotated to a horizontal state to facilitate the mixing to a homogeneous concentration, before being rotated back to a vertical state. At this point, x-ray imaging at 10 s intervals was activated, and continued until the end of the experiment. After at least two hours of following homogeneous temperature and concentration, the bottom heater was turned off to initiate the temperature gradient phase. An x-ray image of such a sample cell is shown in figure 1. The black bends at the top and bottom are the heating wires. One thermocouple is visible at the top and and one at the bottom of the image. In the centre are the four Al-In samples with different compositions, whereby the two samples on the left are demixed, recognisable by the dark area at the bottom of the sample. Of the two remaining samples, one was not properly compressed by the piston, leading to free surfaces, and was thus disregarded from the data set. At least four hours of continuous XRR observation was then allowed. For x-ray imaging we used a micro-focus x-ray source (XT9160-TED, Viscom AG, Hannover, Germany) which was operated at 100 kV and 120 μA, and a CdTe detector with 100 μm pixel size (XC-Thor series, Direct Conversion AB, Danderyd, Sweden). With the sample cell located between the source and detector, the resulting images have a resolution of about 20 pixels per millimetre across the sample. The detector has a range of 4096 grey values, but the weakness of thermodiffusion led to only 10–70 grey values of difference along the sample due to the atomic migration.

To analyse the data from the x-ray images, the grey values of the pixels along each sample are converted to indium concentration using reference material of known concentration, to which a relation between grey value and concentration can be determined [40, 41].

Sedimentation of the denser component is not an issue in atomic fluids while outside of the miscibility gap because the thermal energy is higher than the gravitational potential energy by orders of magnitude [42].

4. Results

The liquid alloys for which experiments were performed are shown in figure 2. The crosses indicate where the XRR imagery revealed that the alloy were inside the miscibility gap, and thus demixed, while the dots show where the alloys were found to not demix, and thus returned valid coefficients.

The concentration along one of these samples, the one of liquid $Al_{85}In_{15}$, is shown at the end of a 2 h isothermal (blue) and at the end of a subsequent 4 h non-isothermal state (orange) in figure 3. The migration of the heavier indium towards the cold side (to the right in the figure) is clearly observed.

The transient concentration separation Δc_{In} for the same sample of liquid $Al_{85}In_{15}$ is shown in the centre column of figure 4. From that figure, it is evident that the sample was not near the steady state by the time the experiment was concluded. The fit of the equation for the transient concentration difference as given by equation (2) (the black curve) returned a Soret coefficient of $S_{\mathrm{T}} = (5.0 \pm 1.4) \times 10^{-3}\,\mathrm{K}^{-1}$ and an interdiffusion coefficient of $D = (1.2 \pm 0.3) \times 10^{-9}\,\mathrm{m}^2\,\mathrm{s}^{-1}$, which gives a thermodiffusion coefficient of $D_{\mathrm{T}} \equiv S_{\mathrm{T}} \times D = (6.1 \pm 2.4) \times 10^{-12}\,\mathrm{m}^2\,\mathrm{s}^{-1}\,\mathrm{K}^{-1}$. For the lower concentration of indium in the sample of $Al_{93.5}In_{6.5}$, the steady state is achieved within the experiment duration, and due to both the

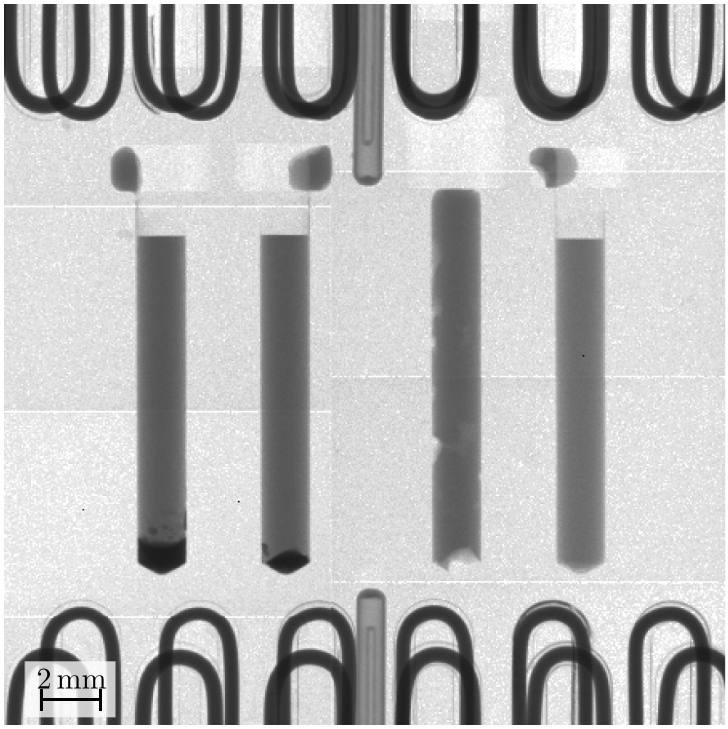

Figure 1. XRR image of a sample cell containing samples of (from left to right) $Al_{87}In_{13.0}$, $Al_{88.8}In_{11.2}$, $Al_{91.1}In_{8.9}$, and $Al_{93.5}In_{6.5}$ at a mean temperature of 1015 K, captured after over 3 h in a temperature gradient. The two samples with the highest indium concentrations were inside the miscibility gap and thus demixed, observed as the dark indium-rich liquid segregated to the bottom due to gravity, while the brighter aluminium-rich liquid is at the top. The piston for the sample of $Al_{91.1}In_{8.9}$ malfunctioned, and consequently free surfaces are visible in that sample. The sample of $Al_{93.5}In_{6.5}$ functioned flawlessly, and neither bubbles nor free surfaces, nor any demixing can be observed.

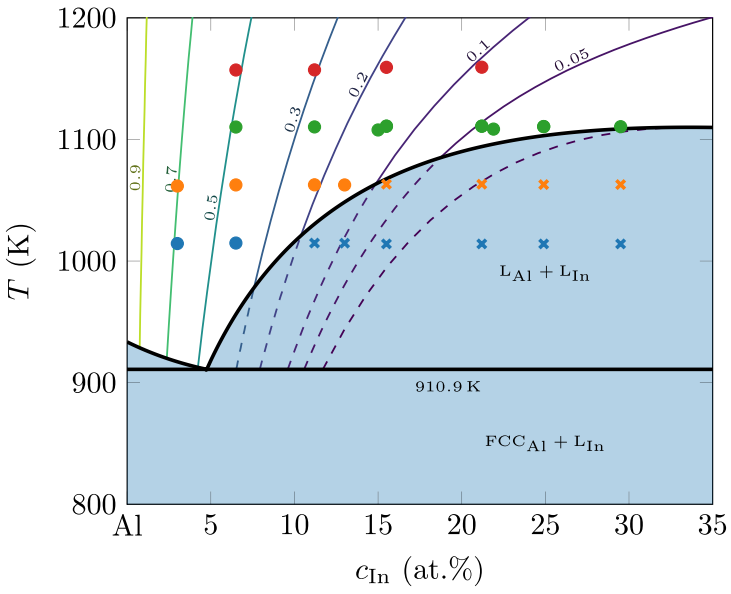

Figure 2. Phase diagram of Al–In with contour lines of the thermodynamic factor, as calculated with the thermodynamic evaluation of Singh and Sommer [23]. The lines are dashed inside the miscibility gap, the innermost line being for $\phi = 0$, also called the spinodal. Where the alloy is solid, the thermodynamic factor is not shown. The coloured dots show the mean concentrations and temperatures of the measured samples, while the crosses show the same for samples which demixed.

lower concentration with the factor $c_0(1 - c_0)$ in equation (1), in addition to the non-diminishing interdiffusion, the concentration separation is much lower than for the sample of $Al_{85}In_{15}$, as is clear in the left column of figure 4. Closer to the critical point, however, the concentration separation is found to be even greater, as is evident in the right column of figure 4, where the transient concentration separation for a sample of $Al_{78.1}In_{21.9}$ is shown.

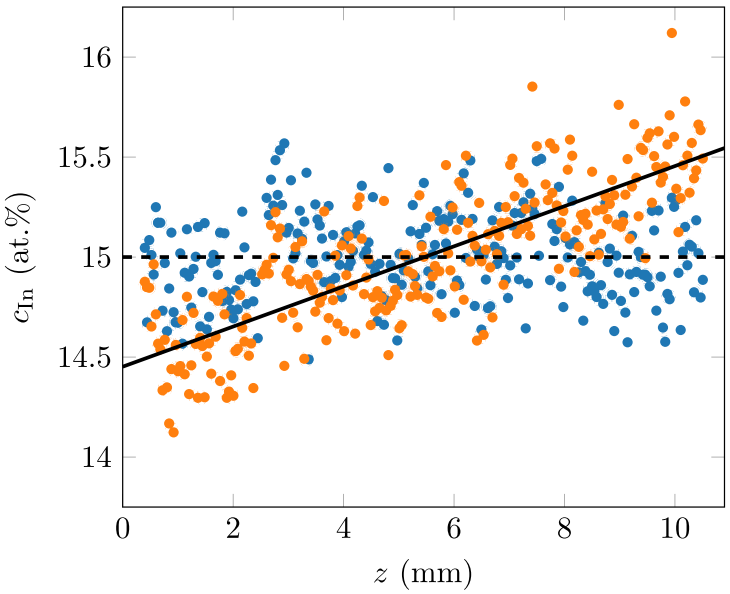

Figure 3. Imaged concentration distribution along a sample of liquid $Al_{85}In_{15}$ without temperature gradient (blue) and after four hours with temperature gradient (orange).

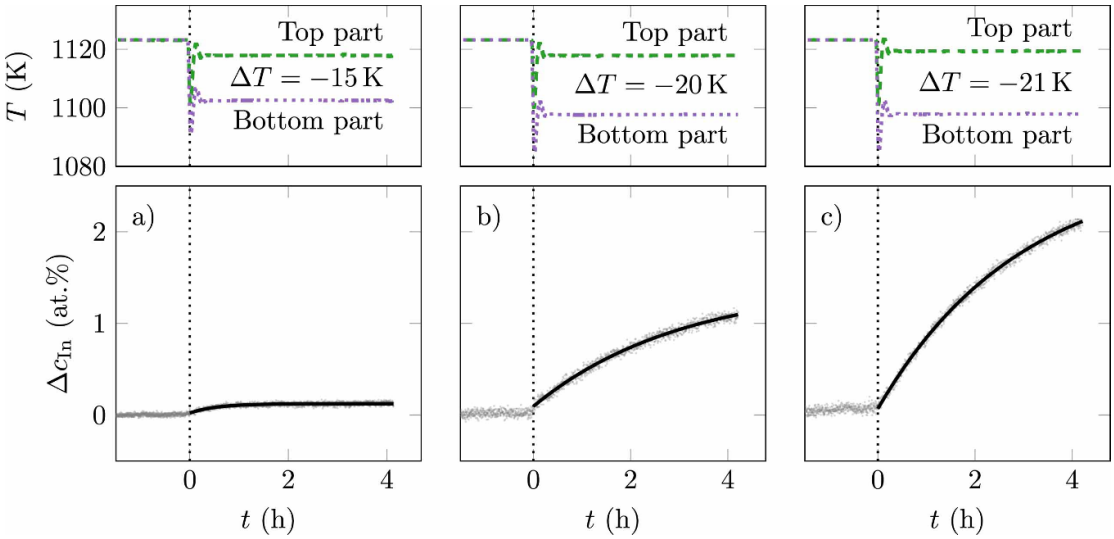

Figure 4. Concentration difference $\Delta c(t)$ along samples of liquid (a) $Al_{93.5}In_{6.5}$, (b) $Al_{85}In_{15}$, and (c) $Al_{78.1}In_{21.9}$ as a function of time, all at a mean temperature of approximately 1110 K. Above, the corresponding temperature at the two ends of the respective sample is shown.

The coefficients from all the experiments are shown in figure 5. For the interdiffusion coefficient, the measurements of Schiller are added for comparison [43], measured at an isothermal temperature using a shear cell furnace in combination with XRR.

The uncertainty in the reported Soret coefficients is mainly from observed random error, in addition to diminishing concentration contrast for the samples with low indium concentration, too short experiment duration leading to difficulty in fitting the exponential equation for the samples with long characteristic times (i.e. for samples with high indium concentration), and measurement error from the thermocouples. Meanwhile, the uncertainties in the reported interdiffusion coefficients are majorly from the observed random error and from the too short experiment duration for the samples with long characteristic times.

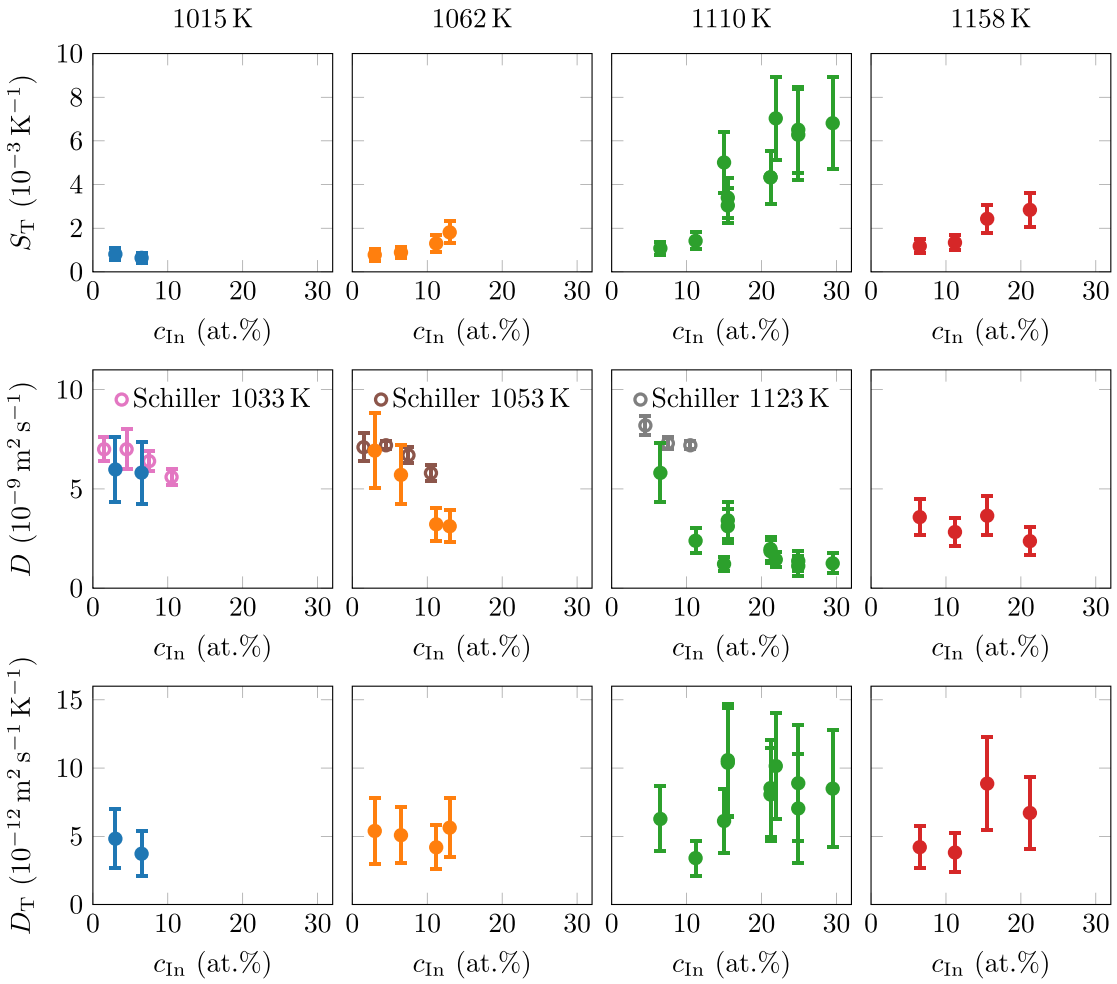

Figure 5. Soret (first row), interdiffusion (second row) and thermodiffusion (third row) coefficients measured for liquid Al–In at mean temperatures of 1015 K (first column, blue), 1062 K (second column, orange), 1110 K (third column, green), and 1158 K (fourth column, red).

5. Discussion

We present a unique data set, where the strong increase of the Soret effect towards the miscibility gap for the first time is measured outside of organic mixtures. In our measurements, the Soret coefficient was found to be always positive for the investigated concentration range. A positive Soret coefficient means that the heavier element (indium) migrated to the colder side, which was previously found to also be the case for Ag–Al [8]. Furthermore, the Soret coefficient was observed to be increasing when the TDF decreased, i.e. when approaching the miscibility gap. Closest to the critical point, which Singh and Sommer places at 1110.0 K at a indium-concentration of 33.6 at% [23], the magnitude of the measured Soret coefficient is observed to be the largest, as seen in the results measured at a mean temperature of 1110 K (green datapoints) in figure 5, while the measurements at lower indium concentrations (measured at 1015 K, blue datapoints, and 1062 K, orange datapoints) or at a higher temperature (1158 K, red datapoints) do not increase as much.

Schiller earlier investigated the interdiffusion in liquid Al–In alloys on the aluminium-rich side [43], where the experiments of this work were also conducted. Using long capillary diffusion couples and XRR, they investigated the interdiffusion coefficient in alloys with the mean concentrations ranging from 1.5 at% to 10.5 at% indium at isothermal temperatures ranging from 953 K to 1273 K. The measurements of liquid $Al_{97}In_3$ from our work were in agreement with the results of Schiller, but for higher indium concentrations, the interdiffusion coefficient was here found to decrease much more pronounced than what was found by Schiller when approaching the miscibility gap. Such a decrease in interdiffusion coefficient closer to the miscibility gap is in agreement with equation (3), and has also been found for other liquid alloys with miscibility gaps [34–36].

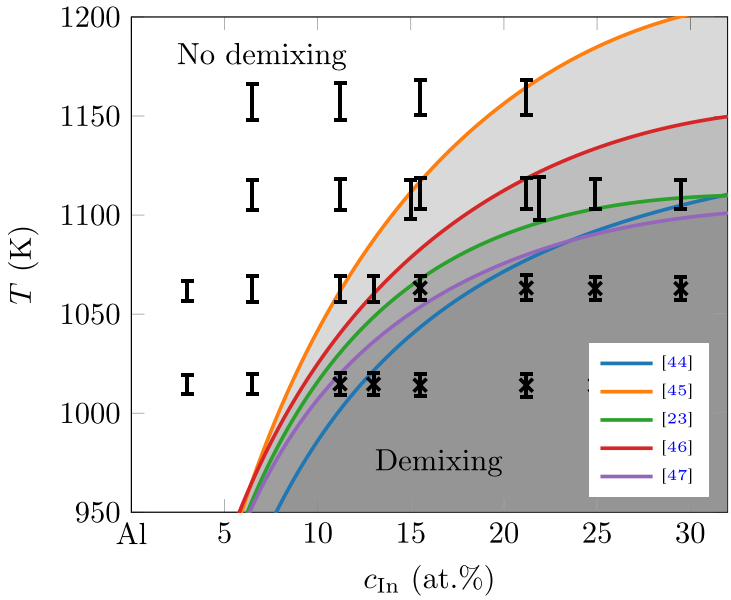

Figure 6. The curves show the different calculated phase diagrams for the Al–In system, calculated from thermodynamic evaluations for which the the reference is indicated in the legend. The bars show the temperature range of each measured sample in this work. A cross is in the bar if the sample was observed to demix while in the given temperature gradient.

In our experiments, while the Soret coefficient and interdiffusion coefficient change by up to an order of magnitude depending on concentration and mean temperature, the thermodiffusion coefficient D_T is remarkably stable for the investigated alloys. This behaviour has also been observed in the investigations of thermodiffusion in organic mixtures [30–32]. While the uncertainty in this measurement is quite high for D_T, the trend is striking: the increase in the Soret coefficient and decrease in the interdiffusion coefficient when closing in on the miscibility gap cancel out for D_T, leaving it practically independent on the change in the TDF when approaching the miscibility gap at higher indium concentration.

Furthermore, we note that the thermodiffusion coefficient measured here is quite similar to the one we measured for liquid Ag–Al at a temperature of 1017 K in an earlier publication of ours, where the thermodiffusion coefficient for liquid $Ag_{30}Al_{70}$, $Ag_{25}Al_{75}$, and $Ag_{20}Al_{80}$ was measured to between $(3.9 \pm 1.0) \times 10^{-12}\,m^2\,s^{-1}\,K^{-1}$ and $(6.0 \pm 1.9) \times 10^{-12}\,m^2\,s^{-1}\,K^{-1}$ for the different Ag–Al alloys, using a similar setup to the one used in this publication [8, 41].

The observation that the interdiffusion and Soret coefficients flatten out at indium concentrations above 20 at% especially for the measurements at 1110 K in figure 5 is not expected, as equation (3) dictates that D should further diminish and S_T further increase as the TDF further approaches zero when closing in to the spinodal. This could indicate that the sample was partly in the miscibility gap, although we argue that such a scenario was clearly visible when it occurred, as seen in the separated samples of figure 1. Demixing on a nano-scale below the resolution of the XRR detector could be argued (in figure 1, 1 pixel is equivalent to roughly 52 μm), but as the demixing when cooling down below the miscibility gap at the end of the experiment was observed to happen rapidly on a macro scale, we find such a hidden sub-pixel demixing unlikely. Another possible explanation for the lack of further change in the coefficients at higher concentrations could be that the rate of interdiffusion is getting so slow in the region close to the spinodal that other disturbances, like convection, are getting more significant for the mass transport, disturbing the measurements. An argument for the validity of the measured Soret and interdiffusion coefficients is the similarity of the measured thermodiffusion coefficient for the different concentrations, hinting to that the alloys from where results are reported in figure 5 were indeed not within the miscibility gap, and could instead mean that the miscibility gap itself (and thus the TDF) is inaccurately modelled by the thermodynamic evaluation in that region of the phase diagram.

The Al–In system is interesting as there is no consensus on where the critical point lies, where critical temperatures from 1103 K to 1209 K have been proposed over the last four decades [23, 44–47]. This disagreement leads to very different thermodynamic evaluations of the liquid, from where the different phase diagrams can be calculated for the concentration range investigated in this work. The resulting phase diagrams are overlaid in figure 6.

During our experiments, demixing was observed with the XRR imagery in a sample of $Al_{88.8}In_{11.2}$ at 1023 K, while a sample of $Al_{84.5}In_{15.5}$ at 1073 K was in a mixed state, but demixed when the bottom heater was turned off, leading the sample temperature to span from 1057 K to 1069 K. The sample of $Al_{70.5}In_{29.5}$ in a temperature gradient spanning from 1103 K to 1118 K was not observed to demix based on the XRR imagery. All these observations are the closest to the evaluation of Singh and Sommer [23], although the mentioned lack of demixing of $Al_{70.5}In_{29.5}$ suggests that the critical temperature should be modelled slightly lower than what they report.

Table 1. List of complete results from the experiments conducted in this work.

c_{In} (at.%)	T (K)	ΔT (K)	S_T (10^{-3} K^{-1})	D (10^{-9} m^2 s^{-1})	D_T (10^{-12} m^2 s^{-1} K^{-1})
3.0	1014	−10	0.8 ± 0.3	6.0 ± 1.6	4.8 ± 2.2
3.0	1062	−10	0.8 ± 0.3	6.9 ± 1.9	5.4 ± 2.4
6.5	1015	−10	0.6 ± 0.2	5.8 ± 1.6	3.7 ± 1.7
6.5	1063	−13	0.9 ± 0.3	5.7 ± 1.5	5.1 ± 2.0
6.5	1110	−15	1.1 ± 0.3	5.8 ± 1.5	6.3 ± 2.4
6.5	1157	−18	1.2 ± 0.3	3.6 ± 0.9	4.2 ± 1.6
11.2	1063	−13	1.3 ± 0.4	3.2 ± 0.8	4.2 ± 1.6
11.2	1110	−16	1.4 ± 0.4	2.4 ± 0.6	3.4 ± 1.3
11.2	1157	−19	1.3 ± 0.4	2.8 ± 0.7	3.8 ± 1.4
13.0	1063	−13	1.8 ± 0.5	3.1 ± 0.8	5.6 ± 2.1
15.0	1108	−20	5.0 ± 1.4	1.2 ± 0.3	6.1 ± 2.4
15.5	1111	−16	3.0 ± 0.8	3.4 ± 0.9	10.4 ± 4.0
15.5	1111	−16	3.4 ± 0.9	3.1 ± 0.9	10.6 ± 4.1
15.5	1159	−18	2.4 ± 0.7	3.7 ± 1.0	8.9 ± 3.4
21.2	1111	−16	4.3 ± 1.2	2.0 ± 0.6	8.5 ± 3.6
21.2	1111	−16	4.3 ± 1.2	1.9 ± 0.6	8.1 ± 3.4
21.2	1159	−18	2.8 ± 0.8	2.4 ± 0.7	6.7 ± 2.7
21.9	1109	−21	7.0 ± 1.9	1.4 ± 0.4	10.2 ± 3.9
24.9	1111	−15	6.3 ± 2.1	1.1 ± 0.5	7.0 ± 4.0
24.9	1111	−15	6.5 ± 2.0	1.4 ± 0.5	8.9 ± 4.3
29.5	1111	−15	6.8 ± 2.1	1.3 ± 0.5	8.5 ± 4.3

6. Conclusion

Thermodiffusion in the liquid binary alloy Al–In has been experimentally investigated at the Al-rich side.

The liquid Al–In system has a miscibility gap, which according to theory and earlier measurements on organic systems implies that the Soret coefficient diverges when closing onto the spinodal. We show that by using *in situ* XRR on Al–In a strong increase in the Soret coefficient near the spinodal can be measured, together with an observed strong decrease in the interdiffusion coefficient. A Soret coefficient of up to $(7.0 \pm 1.9) \times 10^{-3}$ K^{-1} was observed, with indium migrating towards the cold side, which is among the highest Soret coefficients ever measured in a liquid alloy.

Furthermore, by comparing the observed demixing data with the calculated phase diagrams from the different published thermodynamic evaluations, we have shown that the evaluation of Singh and Sommer [23] is the best for the Al–In alloy, as the other calculated phase diagrams do not accurately predict the demixing close to the miscibility gap for concentrations ranging from 10 at% to 15 at% indium.

Acknowledgments

The authors would like to thank their institute workshop for help in manufacturing the setup, and Stephan Schneider for a critical reading of the manuscript.

Data availability statement

The data cannot be made publicly available upon publication because the cost of preparing, depositing and hosting the data would be prohibitive within the terms of this research project. The data that support the findings of this study are available upon reasonable request from the authors.

Table of complete results

The complete results from the experiments in this work are listed in table 1.

ORCID iDs

Asbjørn Torsvik Krüger 0000-0002-3296-0431
Elke Sondermann 0000-0001-5935-8945
Andreas Meyer 0000-0002-0604-5467

References

[1] Srinivasan S and Saghir M Z 2013 *Thermodiffusion in Multicomponent Mixtures* (Springer)
[2] Köhler W and Morozov K I 2016 The Soret effect in liquid mixtures - a review *J. Non-Equilib. Thermodyn.* **41** 151–97
[3] Hsiao H-Y and Chen C 2009 Thermomigration in Pb-free SnAg solder joint under alternating current stressing *Appl. Phys. Lett.* **94** 092107
[4] Ru C Q 2000 Thermomigration as a driving force for instability of electromigration induced mass transport in interconnect lines *J. Mater. Sci.* **35** 5575–9
[5] Sassi M B, Kaddeche S, Lappa M, Millet S, Henry D and Hadid H B 2017 On the effect of thermodiffusion on solute segregation during the growth of semiconductor materials by the vertical Bridgman method *J. Cryst. Growth* **458** 154–65
[6] Lewis J and Huang S 1963 High temperature furnace with a sharp temperature gradient *Rev. Sci. Instrum.* **34** 271–3
[7] Xie D-G, Nie Z-Y, Shinzato S, Yang Y-Q, Liu F-X, Ogata S, Li J, Ma E and Shan Z-W 2019 Controlled growth of single-crystalline metal nanowires via thermomigration across a nanoscale junction *Nat. Commun.* **10** 4478
[8] Krüger A T, Sondermann E and Meyer A 2023 Measurement of the Soret coefficient in liquid Al-Ag alloys using x-ray radiography *Phys. Rev. B* **107** 064301
[9] Bhat B N 1973 *Thermotransport in Liquid Aluminum-Copper Alloys* (NASA TR R-415)
[10] Murarka S P, Kim T Y, Hsieh M Y and Swalin R A 1974 Thermotransport studies in liquid alkali metal alloys *Acta Metall.* **22** 185–9
[11] Williams R K and Philbrook W O 1981 The Soret effect in molten Ag-Te solutions *J. Electrochem. Soc.* **128** 1034–40
[12] Praizey J-P 1989 Benefits of microgravity for measuring thermotransport coefficients in liquid metallic alloys *Int. J. Heat Mass Tran.* **32** 2385–401
[13] Praizey J-P, Van Vaerenbergh S and Garandet J-P 1995 Thermomigration experiment on board EURECA *Adv. Space Res.* **16** 205–14
[14] Kassemi M, Barsi S, Alexander J I D and Banish M 2005 Contamination of microgravity liquid diffusivity measurements by void-generated thermocapillary convection *J. Cryst. Growth* **276** 621–34
[15] Roşu-Pflumm R, Wendl W, Müller-Vogt G, Suzuki S, Kraatz K-H and Frohberg G 2009 Diffusion measurements using the shear cell technique: investigation of the role of Marangoni convection by pre-flight experiments on the ground and during the Foton M2 mission *Int. J. Heat Mass Transf.* **52** 6042–9
[16] Kargl F, Sondermann E, Weis H and Meyer A 2013 Impact of convective flow on long-capillary chemical diffusion studies of liquid binary alloys *High Temp. -High Press.* **42** 3–21
[17] Sondermann E, Kargl F and Meyer A 2019 In situ measurement of thermodiffusion in liquid alloys *Phys. Rev. Lett.* **123** 255902
[18] Mondolfo L F 1976 *Aluminum Alloys: Structure and Properties* (Elsevier) (https://doi.org/10.1016/C2013-0-04239-9)
[19] Dursun T and Soutis C 2014 Recent developments in advanced aircraft aluminium alloys *Mater. Des.* **56** 862–71
[20] Chang Y I 1989 The integral fast reactor *Nucl. Technol.* **88** 129–38
[21] Zhang X-D and Liu J 2020 Perspective on liquid metal enabled space science and technology *Sci. China Technol. Sci.* **63** 1127–40
[22] Liu G L and Liu J 2021 Convective cooling of compact electronic devices via liquid metals with low melting points *J. Heat Transf.* **143** 050801
[23] Singh R N and Sommer F 1997 Segregation and immiscibility in liquid binary alloys *Rep. Prog. Phys.* **60** 57
[24] Ratke L and Diefenbach S 1995 Liquid immiscible alloys *Mater. Sci. Eng. R Rep.* **15** 263–347
[25] Taylor R and Krishna R 1993 *Multicomponent Mass Transfer (Wiley Series in Chemical Engineering)* (Wiley)
[26] Darken L S 1948 Diffusion, mobility and their interrelation through free energy in binary metallic systems *Trans. TMS-AIME* **175** 184–201
[27] Ndjaka A T, García-Fernández L, Bouyou D E B, Lassin A, Azaroual M, Croccolo F and Bataller H 2022 Mass diffusion and Soret coefficient measurements of triethylene glycol/water binary mixtures by dynamic shadowgraphy *Eur. Phys. J. E* **45** 20
[28] Nishida Y, Shimizu M, Okuno T, Matsuoka J, Shimotsuma Y and Miura K 2023 Ultra-high temperature Soret effect in a silicate melt: SiO_2 migration to cold side *J. Chem. Phys.* **159** 134504
[29] Thomaes G 1956 Thermal diffusion near the critical solution point *J. Chem. Phys.* **25** 32–33
[30] Story M J and Turner J C R 1969 Flow-cell studies of thermal diffusion in liquids. Part 5.—Binary mixtures of CH_3OH with CCl_4, benzene and cyclohexane at 25°C *Trans. Faraday Soc.* **65** 1523–9
[31] Giglio M and Vendramini A 1975 Thermal-diffusion measurements near a consolute critical point *Phys. Rev. Lett.* **34** 561–4
[32] Enge W and Köhler W 2004 Thermal diffusion in a critical polymer blend *Phys. Chem. Chem. Phys.* **6** 2373–8
[33] Voit A, Krekhov A, Enge W, Kramer L and Köhler W 2005 Thermal patterning of a critical polymer blend *Phys. Rev. Lett.* **94** 214501
[34] Khairulin R A, Stankus S V and Sorokin A L 2002 Determination of the two-melt phase boundary and study of the binary diffusion in liquid Bi–Ga system with a miscibility gap *J. Non-Cryst. Solids* **297** 120–30
[35] Abdellah A B, Gasser J G, Bouziane K, Grosdidier B and Busaidi M 2007 Experimental procedure to determine the interdiffusion coefficient of miscibility gap liquid alloys: case of GaPb system *Phys. Rev. B* **76** 174203
[36] Khairulin R A, Abdullaev R N and Stankus S V 2019 Phase equilibria and mutual diffusion in liquid lithium–sodium alloys *J. Eng. Thermophys.* **28** 472–83
[37] Costesèque P, Pollak T, Platten J K and Marcoux M 2004 Transient-state method for coupled evaluation of Soret and Fick coefficients and related tortuosity factors, using free and porous packed thermodiffusion cells: Application to CuSO4 aqueous solution (0.25M) *Eur. Phys. J. E* **15** 249–53

[38] de Groot S R and Mazur P 1962 *Non-Equilibrium* (Dover Publications, Inc)
[39] Hartung M 2007 A detailed treatment of the measurement of transport coefficients in transient grating experiments *PhD Thesis* University of Bayreuth (available at: https://epub.uni-bayreuth.de/id/eprint/667/)
[40] Griesche A, Zhang B, Solórzano E and Garcia-Moreno F 2010 Note: x-ray radiography for measuring chemical diffusion in metallic melts *Rev. Sci. Instrum.* **81** 056104
[41] Krüger A T 2025 Thermodiffusion in liquid binary and ternary alloys *Phdthesis* (Ruhr-University Bochum)
[42] Sondermann E, Voigtmann T and Meyer A 2022 Influence of gravity on atomic mobility in a liquid *Microgravity Sci. Technol.* **34** 93
[43] Schiller T 2022 Further development of radiographic in situ interdiffusion experiments and investigation of (quasi-)binary Al-rich melts *PhD Thesis* (Ruhr–University)
[44] Murray J L 1983 The Al-In (aluminum-indium) system *Bull. Alloy Phase Diagr.* **4** 271–8
[45] Ansara I *et al* 1994 A binary database for III-V compound semiconductor systems *Calphad* **18** 177–222
[46] Kim S S and Sanders T H 2006 Thermodynamic assessment of the metastable liquidi in the Al-In, Al-Bi and Al-Pb systems *Model. Simul. Mater. Sci. Eng.* **14** 1181
[47] Kaban I, Curiotto S, Chatain D and Hoyer W 2010 Surfaces, interfaces and phase transitions in Al-In monotectic alloys *Acta Mater.* **58** 3406–14